

On the Role of Metastable States in Low Pressure Oxygen Discharges

J. T. Gudmundsson^{1,2,a)} and H. Hannesdóttir¹

¹*Science Institute, University of Iceland, Dunhaga 3, IS-107 Reykjavik, Iceland*

²*Department of Space and Plasma Physics, School of Electrical Engineering, KTH – Royal Institute of Technology, SE-100 44, Stockholm, Sweden*

^{a)}Corresponding author: tumi@hi.is

Abstract. We use the one-dimensional object-oriented particle-in-cell Monte Carlo collision code oopd1 to explore the spatio-temporal evolution of the electron heating mechanism in a capacitively coupled oxygen discharge in the pressure range 10 – 200 mTorr. The electron heating is most significant in the sheath vicinity during the sheath expansion phase. We explore how including and excluding detachment by the singlet metastable states $O_2(a^1\Delta_g)$ and $O_2(b^1\Sigma_g^+)$ influences the heating mechanism, the effective electron temperature and electronegativity, in the oxygen discharge. We demonstrate that the detachment processes have a significant influence on the discharge properties, in particular for the higher pressures. At 10 mTorr the time averaged electron heating shows mainly ohmic heating in the plasma bulk (the electronegative core) and at higher pressures there is no ohmic heating in the plasma bulk, that is electron heating in the sheath regions dominates.

INTRODUCTION

Capacitively coupled plasma (CCP) radio frequency discharges are frequently used for applications such as plasma etching or plasma enhanced chemical vapor deposition (PECVD) processes in integrated circuit manufacturing. Impact by energetic electrons leads to dissociation and ionization of feedstock gas, and thus creation of reactive radicals and ions. These applications usually require feedstock gases that are complex mixtures of reactive gases, often electronegative. One such electronegative discharge is the oxygen discharge. The oxygen discharge and its mixtures are of significance in various materials processing applications including etching of polymer films, ashing of photoresist, oxidation, and deposition of oxide films. The oxygen chemistry is complicated due to the presence of metastable atomic and molecular species. It is in particular the two low lying metastable molecular states designated by $a^1\Delta_g$ and $b^1\Sigma_g^+$, which are located 0.98 and 1.627 eV above the ground state, respectively, that play an important role. It is well established that collisions with these metastable states have in many cases larger cross sections and thus higher reaction rates than corresponding collisions with the ground state molecule.

A volume averaged global model is an approach to get a detailed description of the plasma chemistry in low pressure discharges. Global model studies show that the dominant species in the oxygen discharge is the oxygen molecule in the ground state, $O_2(X^3\Sigma_g^-)$, followed by the oxygen atom in the ground state, $O(^3P)$. The singlet metastable states $O_2(a^1\Delta_g)$ and $O_2(b^1\Sigma_g^+)$ and the metastable atom $O(^1D)$ are also present in the plasma in significant amounts [1, 2, 3]. Furthermore, a recent study shows that the $O_2(b^1\Sigma_g^+)$ density can overcome the $O_2(a^1\Delta_g)$ density in the pressure range below 100 mTorr [3]. The O_2^+ -ions are in majority among the positive ions and the O^+ -ion density is much smaller and has a sharp decrease for pressures above 4 mTorr. It is also seen that the negative ion density ratio $[O^-]/[O_2^-]$ is 5.3 at 1 mTorr, and 1.3 at 100 mTorr [3]. Such global models neglect spatial variations in the plasma parameters as well as the kinetics of the discharge. They allow us to explore the relative reaction rates for the creation and destruction of particular species over the pressure range of interest and therefore which reactions are of significance.

To explore the kinetics of the discharge we apply particle-in-cell Monte Carlo collision (PIC/MCC) simulations. In a PIC/MCC simulation the plasma is represented as a collection of macro-particles. Equations of motion are solved for each macro-particle. The electric and magnetic fields are calculated self-consistently using charge densities and currents produced by these macro-particles. We use the oopd1 (object oriented plasma device for one dimension)

code to simulate the discharge. It has one dimension in space and three velocity components for the particles (1d-3v). The oopd1 code is supposed to replace the widely used xpd1 series (xpd1, xpd1c and xpd1s). It was developed to simulate various types of plasmas, including processing discharges, accelerators and beams. The code is written in modular structure and it includes features such as relativistic kinematics and different weights for different species. Earlier we developed a basic oxygen discharge model and benchmarked it against the well known xpd1 code [4]. Later we explored adding the singlet metastable molecule $O_2(a^1\Delta_g)$ and the metastable oxygen atom $O(^1D)$ to the reaction set [5]. There we demonstrated that the addition of the singlet metastable molecule $O_2(a^1\Delta_g)$ has a significant influence on the discharge, such as on the electronegativity, the effective electron temperature, and the electron heating processes for a pressure of 50 mTorr. We found that it is, in particular, detachment by the metastable molecule $O_2(a^1\Delta_g)$ that has a significant influence on the discharge properties. In a subsequent study we explored how the addition of the singlet metastable molecule $O_2(a^1\Delta_g)$ modified the discharge properties in the pressure range 10 – 500 mTorr [6]. We found that at low pressure (10 mTorr), ohmic (collisional) heating in the plasma bulk dominates and the heating mechanism evolves through a phase where both ohmic heating in the bulk and sheath oscillation (collisionless) heating contribute, and at higher pressure (50 – 500 mTorr), the electron heating occurs almost solely in the sheath region. At the higher pressures, detachment by the metastable singlet molecule $O_2(a^1\Delta_g)$ has a significant influence on the electron heating process but at the lowest pressures detachment by $O_2(a^1\Delta_g)$ has only a small influence on the heating process. At low pressure, the electron energy probability function (EPPF) is convex and as the pressure is increased the number of low energy electrons increases and the number of higher energy electrons (> 10 eV) decreases, and the EPPF develops a concave shape or becomes bi-Maxwellian [6]. This contradicts what is observed for a capacitively coupled argon discharge where the EPPF evolves from being concave at low pressure to become convex at high pressure [7, 8] and for the chlorine discharge where the EPPF is found to be convex in the pressure range of 10 – 100 mTorr [9]. In a more recent study we added the singlet metastable oxygen molecule $O_2(b^1\Sigma_g^+)$ to the reaction set [10]. We find that including the singlet metastable $O_2(b^1\Sigma_g^+)$ further decreases the ohmic heating in the electronegative core and the effective electron temperature in the bulk region. The effective electron temperature in the electronegative core is found to be less than 1 eV in the pressure range 50 – 200 mTorr which agrees with recent experimental findings. Furthermore, we have added an energy-dependent secondary electron emission yield for the positive oxygen ions O_2^+ and O^+ as well as the neutrals O_2 and O [10]. We find that including an energy-dependent secondary electron emission yield for O_2^+ -ions has a significant influence on the discharge properties, including decreased sheath width and increased electron density [10]. Other PIC/MCC studies of the oxygen discharge have also indicated a significant role of the singlet metastable state $O_2(a^1\Delta_g)$ and in particular the detachment by the $O_2(a^1\Delta_g)$ on the overall discharge properties [11, 12]. However, these studies did not include a complete reaction set for creation and destruction of the metastable states and the metastables are not treated kinetically.

Here, we investigate the spatio-temporal electron heating dynamics in a geometrically symmetric oxygen discharge by 1d-3v PIC/MCC simulations. In particular we explore the influence of the electron detachment from the negative ion O^- by the singlet molecular metastables $O_2(a^1\Delta_g)$ and $O_2(b^1\Sigma_g^+)$ on the spatio-temporal electron heating dynamics, the electronegativity, and the effective electron temperature.

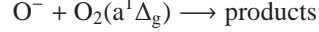
THE SIMULATION AND THE OXYGEN DISCHARGE

We assume a capacitively coupled discharge where one of the electrodes is driven by an rf voltage (left hand electrode) while the other (right hand electrode) is grounded. We assume the discharge to be operated at a single frequency of 13.56 MHz, and voltage amplitude of $V_0 = 222$ V with an electrode separation of 4.5 cm and a capacitor of 1 F in series with the voltage source. The simulation grid is uniform and consists of 1000 cells. The electron time step is 3.68×10^{-11} s. The simulation was run for 5.5×10^6 time steps or 2750 rf cycles. For the heavy particles we use sub-cycling and the heavy particles are advanced every 16 electron time steps [13]. We assume that the initial density profiles are parabolic.

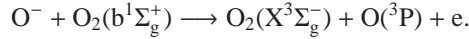
The oxygen discharge

We consider an oxygen discharge that consists of: electrons, the ground state oxygen molecule $O_2(X^3\Sigma_g^-)$, the metastable oxygen molecules $O_2(a^1\Delta_g)$, and $O_2(b^1\Sigma_g^+)$, the ground state oxygen atom $O(^3P)$, the metastable oxygen atom $O(^1D)$, the negative oxygen ion O^- , and the positive oxygen ions O^+ and O_2^+ . The basic reaction set and cross sections included in the oopd1 code for the oxygen discharge excluding the metastable states is discussed in an

earlier work and includes reactions among electrons, ground state molecules, ground state atoms, negative ions O^- , and positive ions O^+ and O_2^+ [4]. Similarly, the reactions and cross sections involving the metastable oxygen atom $O(^1D)$ and the metastable oxygen molecule $O_2(a^1\Delta_g)$ are discussed by Gudmundsson and Lieberman [5]. The reactions involving the metastable singlet molecule $O_2(b^1\Sigma_g^+)$, that are included in the model, and the energy dependent secondary electron emission yields are discussed by Hannesdottir and Gudmundsson [10]. The combined reaction set discussed in these three publications [4, 5, 10] is referred to as the full reaction set in the discussion below. The reactions explored here in particular are detachment by the singlet metastable molecule $O_2(a^1\Delta_g)$



and detachment by the metastable $O_2(b^1\Sigma_g^+)$



For the detachment by the metastable $O_2(a^1\Delta_g)$ we use the rate coefficient measured at 400 K of $1.5 \times 10^{-16} \text{ m}^2/\text{s}$ by Midey et al. [14] to estimate the cross section, which is allowed to fall as $\sim 1/\sqrt{E}$, where E is the energy, to 184 meV and then take a fixed value of $5.75 \times 10^{-20} \text{ m}^2$. Also we assume that detachment by the metastable $O_2(a^1\Delta_g)$ leads to the formation of $O(^3P) + O_2(X^3\Sigma_g^-) + e$, instead of $O_3 + e$ and $O + O_2^-$. The cross section for detachment from O^- by $O_2(b^1\Sigma_g^+)$ is estimated from the rate coefficient of $6.9 \times 10^{-16} \text{ m}^3/\text{s}$, given by Aleksandrov [15] and then we allow it to fall as $\sim 1/\sqrt{E}$ for $E < 184 \text{ meV}$ and then remain constant.

The neutral gas density is much higher than the densities of charged species, so the neutral species at thermal energies (below a certain cut-off energy) are treated as a background with fixed density and temperature and maintained uniformly in space. These neutral background species are assumed to have a Maxwellian velocity distribution at the gas temperature (here $T_n = 26 \text{ mV}$). In the oxygen discharge, the densities of the metastable oxygen molecules $O_2(a^1\Delta_g)$ and $O_2(b^1\Sigma_g^+)$, oxygen atom in the ground state $O(^3P)$ and the metastable oxygen atom $O(^1D)$ are much larger than the number of charged species. We assume that the background consists of 4.4 % $O_2(a^1\Delta_g)$, 4.4 % $O_2(b^1\Sigma_g^+)$, 90.6 % $O_2(X^3\Sigma_g^-)$, 0.519 % $O(^3P)$ and 0.028 % $O(^1D)$ as in our earlier work [10]. The neutrals are treated kinetically as particles if their energy exceeds a preset threshold value. The threshold values used here for the neutral species are listed in table 1. As a neutral species hits the electrode it returns as a thermal particle with a given probability and atoms can recombine to form a thermal molecule with the same probability. These wall recombination probabilities as well as the quenching coefficients used for the excited neutral species are listed in table 1. The choice of the quenching coefficients for the molecular metastables and its influence on the discharge properties is discussed towards the end of next section. The secondary electron emission yield for O_2^+ , O^+ -ions, O_2 molecules and O atoms are energy dependent and we used the fits for oxidized metal given elsewhere [10].

TABLE 1. The parameters of the simulation, the particle weight, the threshold above which the dynamics of the neutral particles are followed and the wall recombination and quenching coefficients used.

Species	particle weight	threshold [meV]	wall quenching or recombination coefficient
$O_2(X^3\Sigma_g^-)$	5×10^7	500	1.0
$O_2(a^1\Delta_g)$	5×10^7	100	0.007 [16]
$O_2(b^1\Sigma_g^+)$	5×10^7	100	0.1 (see text)
$O(^3P)$	5×10^8	500	0.5
$O(^1D)$	5×10^8	50	1.0 (0.5 recomb., 0.5 quenching)
O_2^+	10^7	-	-
O^+	10^6	-	-
O^-	5×10^6	-	-
e	1×10^8	-	-

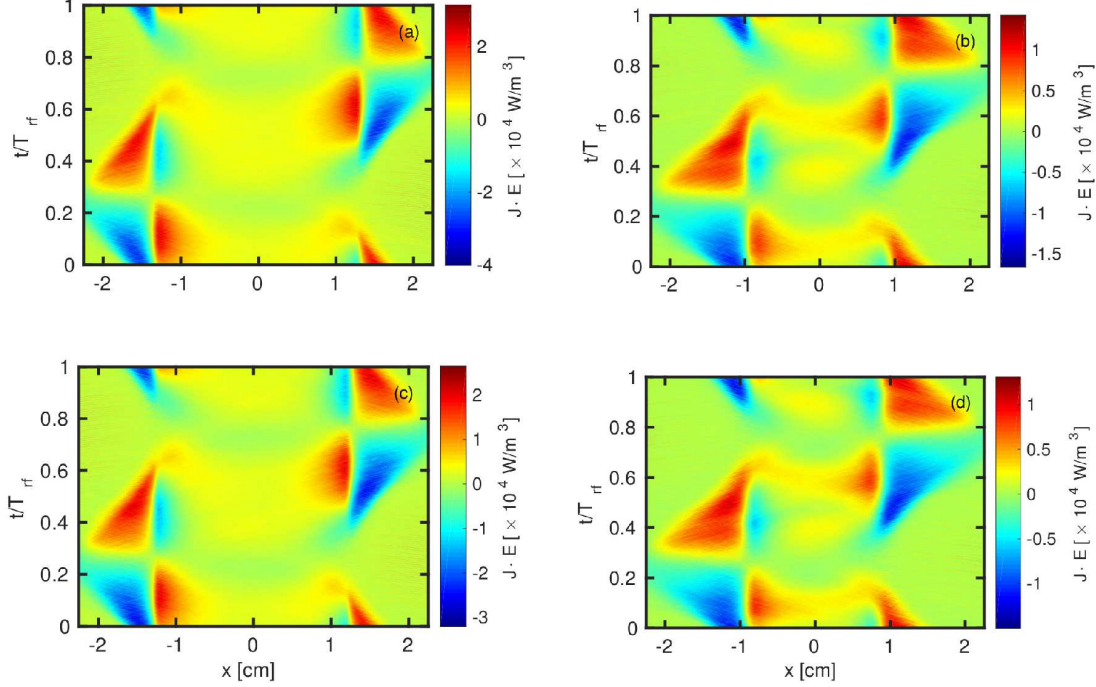


FIGURE 1. The electron heating profile for a parallel plate capacitively coupled oxygen discharge at 10 mTorr with a gap separation of 4.5 cm driven by a 222 V voltage source at 13.56 MHz. The four cases explored are: (a) detachment neither by $O_2(a^1\Delta_g)$ nor $O_2(b^1\Sigma_g^+)$, (b) only detachment by $O_2(b^1\Sigma_g^+)$ included, (c) only detachment by $O_2(a^1\Delta_g)$ included, (d) and both detachment by $O_2(a^1\Delta_g)$ and $O_2(b^1\Sigma_g^+)$ included (full reaction set).

RESULTS AND DISCUSSION

The electron power absorption is calculated as $\mathbf{J}_e \cdot \mathbf{E}$, where \mathbf{J}_e and \mathbf{E} are the spatially and temporally varying electron current density and electric field, respectively. The spatio-temporal behavior of the electron power absorption, for pressures 10, 50 and 200 mTorr, is shown in figures 1 – 3, respectively, for four cases, (a) when the detachment by both the metastable states $O_2(a^1\Delta_g)$ and $O_2(b^1\Sigma_g^+)$ are neglected, (b) when detachment by $O_2(a^1\Delta_g)$ is neglected and by $O_2(b^1\Sigma_g^+)$ is included, (c) when detachment by $O_2(a^1\Delta_g)$ is included and by $O_2(b^1\Sigma_g^+)$ is neglected, and (d) when the detachments by both the metastable states $O_2(a^1\Delta_g)$ and $O_2(b^1\Sigma_g^+)$ are included in the simulations (the full reaction set). For each of the figures the abscissa covers the whole inter-electrode gap, from the powered electrode on the left hand side to the grounded electrode on the right hand side. Similarly the ordinate covers the full rf cycle. The four figures grouped together for each pressure value can have different magnitude scales. Therefore, there can be differences in the four figures, not only qualitatively but also quantitatively. When comparing the figures for each pressure be aware of such subtle differences. Figure 1 (a) shows the spatio-temporal behavior of the electron power absorption at 10 mTorr when the detachments by both the metastable states $O_2(a^1\Delta_g)$ and $O_2(b^1\Sigma_g^+)$ are neglected in the simulation. The most significant heating is in the sheath region, however there is a significant contribution to the heating in the bulk region. Both energy gain (red and yellow areas) and energy loss (dark blue areas) are evident. As detachment by $O_2(b^1\Sigma_g^+)$ only is added to the simulation in figure 1 (b) the spatio-temporal heating structure is maintained but the sheath width increases. Note that there is also a change in the scale when detachment by $O_2(b^1\Sigma_g^+)$ is added, the peak electron heating in the sheath region decreases. Adding detachment by $O_2(a^1\Delta_g)$ only does not lead to decreased sheath with as seen in figure 1 (c). Including both the detachment processes (the full reaction set) shows very similar spatio-temporal heating structure as when only $O_2(b^1\Sigma_g^+)$ is included in the simulation. In all cases the electron heating is most significant during the sheath expansion phase at each electrode (the red areas). We also observe electron heating during the sheath collapse on the bulk side of the sheath edge while there is cooling

(electrons loose energy) on the electrode side (the lower left hand corner and upper center on the right hand side). This is in accordance to what is commonly observed in single frequency capacitively coupled discharges [17]. Setting the electron emission coefficient to zero gives almost exactly the same spatio-temporal heating structure for all the four cases (not shown). The spatio-temporal heating structure at 50 mTorr is shown in figure 2. When detachment by both the metastable states is neglected there is significant heating in the electronegative core as seen in figure 2 (a) (green and yellow areas). When detachment by the singlet state $O_2(a^1\Delta_g)$ only is included, the heating in the electronegative core decreases as seen in figure 2 (c) but when detachment by the singlet state $O_2(b^1\Sigma_g^+)$ only is included the heating in the electronegative core decreases more or to almost zero as seen in figure 2 (b). Including both the detachment processes (the full reaction set) shows almost zero heating in the electronegative core as seen in figure 2 (d). In all cases the electron heating is most significant during the sheath expansion phase at each electrode (the red areas). We note oscillations in the heating like those reported by Vender and Boswell [18] as we add detachment by the singlet metastable molecules to the simulations. We also note that cooling in the sheath region during the sheath collapse is always apparent (note the different scale). At 200 mTorr when detachment by both the metastable states

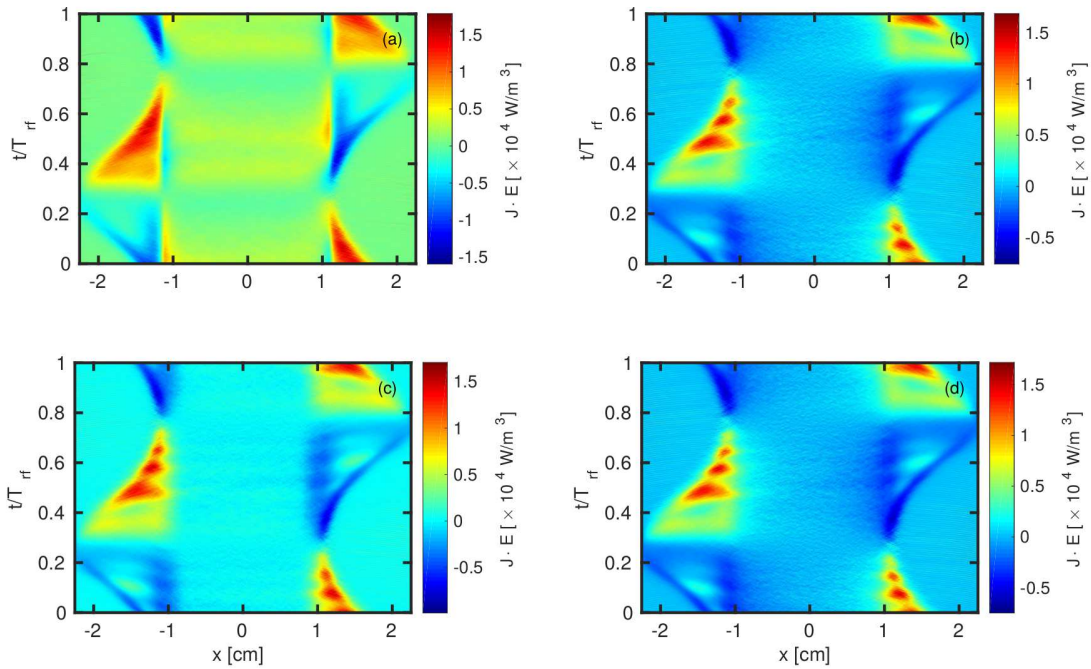


FIGURE 2. The electron heating profile for a parallel plate capacitively coupled oxygen discharge at 50 mTorr with a gap separation of 4.5 cm driven by a 222 V voltage source at 13.56 MHz. The four cases explored are: (a) detachment neither by $O_2(a^1\Delta_g)$ nor $O_2(b^1\Sigma_g^+)$, (b) only detachment by $O_2(b^1\Sigma_g^+)$ included, (c) only detachment by $O_2(a^1\Delta_g)$ included, (d) and both detachment by $O_2(a^1\Delta_g)$ and $O_2(b^1\Sigma_g^+)$ included (full reaction set).

is neglected there is still a significant heating in the electronegative core as seen in figure 3 (a). When detachment by either $O_2(a^1\Delta_g)$ or $O_2(b^1\Sigma_g^+)$ is included in the simulation the heating in the electronegative core drops to zero, as seen in figures 3 (c) and 3 (b), respectively. As a consequence including both the detachment processes shows almost zero heating in the electronegative core as seen in figure 3 (d). In all cases the electron heating is most significant during the sheath expansion phase at each electrode (the red areas). Greb et al. [19] find that at 300 mTorr ohmic (collisional) heating is the dominant heating mechanism far exceeding collisionless heating. They see that collisional electron heating has the highest contribution close to the sheath edge, during the sheath expansion and sheath collapse phases. They also find that collisionless electron heating has higher contribution at the sheath edge during sheath expansion than collisional heating. For collisionless heating they find high negative electron heating (or cooling) at the sheath edge during the sheath collapse phase.

Figure 4 (a) shows the time averaged electron heating profile at 10, 50 and 200 mTorr for the four cases explored here. At 10 mTorr the electron heating is mainly ohmic heating in the electronegative core. This bulk heating decreases

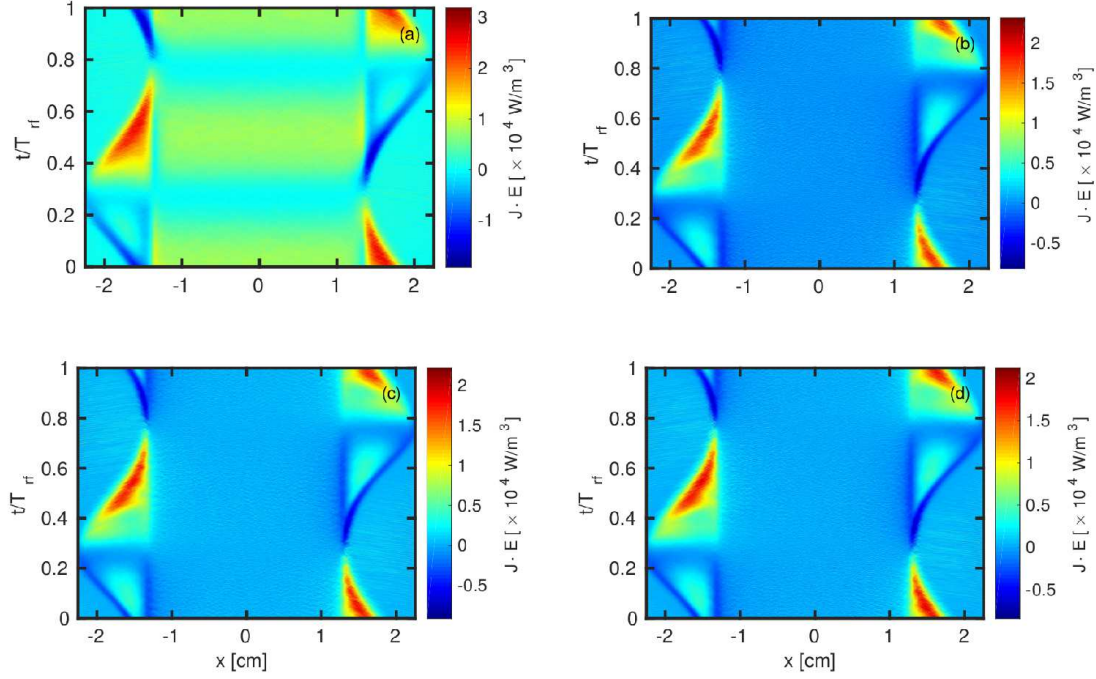


FIGURE 3. The electron heating profile for a parallel plate capacitively coupled oxygen discharge at 200 mTorr with a gap separation of 4.5 cm driven by a 222 V voltage source at 13.56 MHz. The four cases explored are: (a) detachment neither by $O_2(a^1\Delta_g)$ nor $O_2(b^1\Sigma_g^+)$, (b) only detachment by $O_2(b^1\Sigma_g^+)$ included, (c) only detachment by $O_2(a^1\Delta_g)$ included, (d) and both detachment by $O_2(a^1\Delta_g)$ and $O_2(b^1\Sigma_g^+)$ included (full reaction set).

only slightly when detachment is by $O_2(a^1\Delta_g)$ only is added to the reaction set, but decreases more significantly when detachment by $O_2(b^1\Sigma_g^+)$ only is included in the reaction set. Having the full reaction set in the simulation gives almost the same electron heating rate profile as when detachment by $O_2(b^1\Sigma_g^+)$ only is included. Note that when we neglect the detachment by the metastables there is effective cooling in the sheath region during one period as seen in figure 4 (a). This is due to very strong cooling in the sheath collapse phase as seen in figure 1 (a). The strong heating in the sheath region during the sheath expansion of the rf cycle is not significant enough to overcome this cooling during one period. When both detachment processes are included these cooling and heating phases balance and there is almost no effective heating in the sheath regions. At 50 mTorr the ohmic heating in the electronegative core is significant when detachment by the singlet metastables is neglected. However, ohmic heating in the electronegative core drops to almost zero when either detachment by $O_2(a^1\Delta_g)$ or $O_2(b^1\Sigma_g^+)$ is included in the simulation. Detachment by $O_2(b^1\Sigma_g^+)$ only has slightly stronger influence on the ohmic heating in the electronegative core. At 200 mTorr there is a significant ohmic heating in the electronegative core when detachment by both the singlet metastables is neglected and it drops to almost zero when either detachment by $O_2(a^1\Delta_g)$ or $O_2(b^1\Sigma_g^+)$ is included in the simulation. The peak electron heating in the sheath region is higher at 200 mTorr than at 50 mTorr. The same is seen when exploring the effective electron temperature profile shown in figure 4 (b). The effective electron temperature profile changes significantly when detachment by singlet metastables is added to the reaction set. At 10 mTorr detachment by $O_2(a^1\Delta_g)$ only has small effect on the effective electron temperature while detachment by $O_2(b^1\Sigma_g^+)$ only decreases the effective electron temperature significantly. At 50 mTorr detachment by both $O_2(a^1\Delta_g)$ and $O_2(b^1\Sigma_g^+)$ lowers the effective electron temperature but detachment by $O_2(b^1\Sigma_g^+)$ has more influence. At 200 mTorr including either one of the detachment processes is enough to get the same value of the effective electron temperature as when the full reaction set is used in the simulations. This low effective electron temperature in the discharge center indicates that the heating of the electrons is effective in the sheath region, but the ohmic (or collisional) heating in the discharge center is ineffective. The effective electron temperature when the full reaction set is assumed in the simulations is in accordance with the measurements of Kechkar [20] which find $T_{\text{eff}} < 1$ eV in the pressure range 50 - 200 mTorr

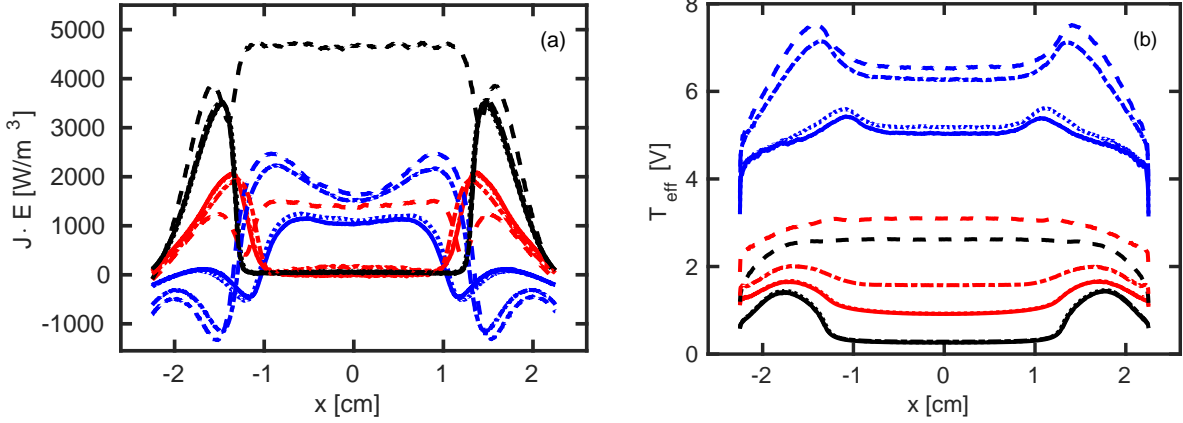


FIGURE 4. (a) The electron heating rate profile and (b) the effective electron temperature profile for a parallel plate capacitively coupled oxygen discharge at 10 (blue), 50 (red) and 200 (black) mTorr with a gap separation of 4.5 cm driven by a 222 V voltage source at 13.56 MHz. The four cases explored are: detachment neither by $O_2(a^1\Delta_g)$ nor $O_2(b^1\Sigma_g^+)$ (dashed line), only detachment by $O_2(b^1\Sigma_g^+)$ included (dotted line), only detachment by $O_2(a^1\Delta_g)$ included (dash-dot line), and both detachment by $O_2(a^1\Delta_g)$ and $O_2(b^1\Sigma_g^+)$ included (full reaction set) (solid line).

in a slightly asymmetric discharge in pure oxygen. Furthermore, Pulpytel et al. [21] measured the effective electron temperature in an Ar/ O_2 (1:3) mixture at 110 mTorr and voltages above 300 V to be around 1 eV.

Figure 5 (a) shows the center electronegativity $\alpha_0 = n_-/n_{e0}$ where n_- is the center negative ion density and n_{e0} is the center electron density. The negative ions are confined to the plasma bulk due to a potential well, and the negative ion density has a peak near the discharge center. We see that the center electronegativity decreases with increasing discharge pressure. Stoffels et al. [22] measure the electronegativity to be in the range 5 – 10 and find it to decrease with increased pressure. This is somewhat higher electronegativity than what we show here. The pressure dependence contradicts the findings reported by Bera et al. [23] which apply a PIC/MCC hybrid model to a low pressure oxygen discharge, and observe an increase in electronegativity with increased pressure. As seen in figure 5 (a) the electronegativity decreases as we add detachment processes to the discharge model. Adding detachment by $O_2(b^1\Sigma_g^+)$ has more significant influence on the electronegativity than adding detachment by $O_2(a^1\Delta_g)$. The average electronegativity is given as

$$\alpha_{ave} = \frac{\int_0^d n_-(x) dx}{\int_0^d n_e(x) dx} \quad (1)$$

where n_- is the O^- -ion density, n_e is the electron density and d is the electrode separation. We see that the average electronegativity shown in figure 5 (b) is always somewhat lower than the center electronegativity. Earlier we explored the influence of increasing the singlet molecular metastable $O_2(a^1\Delta_g)$ density on the electron heating rate. We find that increasing the partial pressure of the metastable molecule $O_2(a^1\Delta_g)$ in the background does not have much influence on the electron heating except that the ohmic heating in the bulk is closer to zero and the electronegativity is slightly lower when 8.8 % of the discharge pressure is due to the metastable molecule $O_2(a^1\Delta_g)$ [6]. Similarly increasing the partial pressure of $O_2(b^1\Sigma_g^+)$ decreases the electronegativity even further [10]. But for a change in partial pressure of $O_2(b^1\Sigma_g^+)$ from 2.2 % to 4.4 % there is not a significant change in electronegativity. It has been demonstrated by using a 1D fluid model that the electronegativity depends strongly on the $O_2(a^1\Delta_g)$ surface quenching probability [19]. For this current study we use a quenching probability of 0.007 estimated by Sharpless and Slanger [16] for iron. Their estimate for aluminum is $< 10^{-3}$. Greb et al. [19] argue that increased quenching coefficient leads to decreased $O_2(a^1\Delta_g)$ density and thus decreased detachment by the $O_2(a^1\Delta_g)$ state and thus higher negative ion density. For iron Ryskin and Shub [24] report a value of 0.0044 and, for aluminum, 5×10^{-5} . Aluminum electrodes would therefore lead to higher singlet metastable densities and lower electronegativity. We have seen in global model studies that wall quenching can be the main loss mechanism for the singlet metastable state $O_2(b^1\Sigma_g^+)$ [3]. In these studies we assumed the quenching coefficient to be 0.1, which is the same value as that assumed in this current study. This assumption is based on the suggestion that the quenching coefficient for the $b^1\Sigma_g^+$ state is about two orders of magnitude larger than

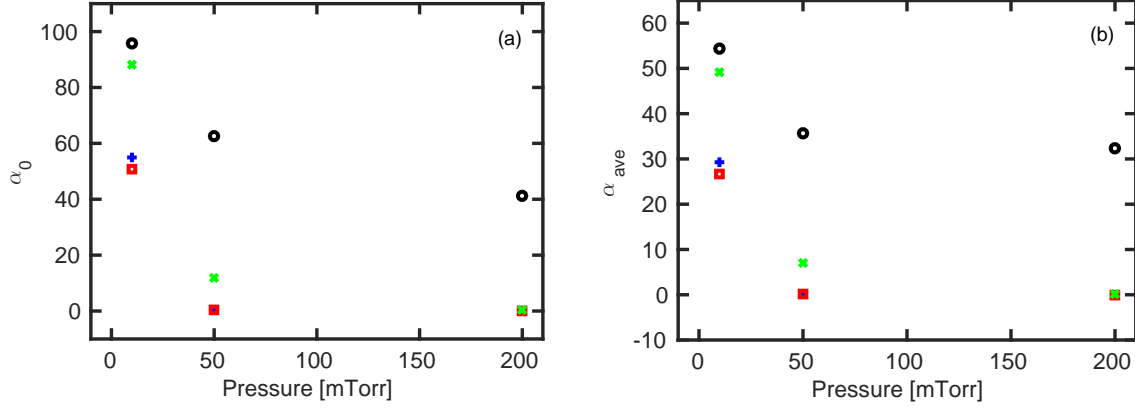


FIGURE 5. (a) The center electronegativity and (b) the average electronegativity as a function of pressure for a parallel plate capacitively coupled oxygen discharge at 50 mTorr with a gap separation of 4.5 cm driven by a 222 V voltage source at 13.56 MHz. The four cases explored are: detachment neither by $O_2(a^1\Delta_g)$ nor $O_2(b^1\Sigma_g^+)$ (\bullet), only detachment by $O_2(a^1\Delta_g)$ included (\times), only detachment by $O_2(b^1\Sigma_g^+)$ included ($+$), and both detachment by $O_2(a^1\Delta_g)$ and $O_2(b^1\Sigma_g^+)$ included (full reaction set) (\square).

that for the $a^1\Delta_g$ state [25].

CONCLUSION

We used the one-dimensional object-oriented particle-in-cell Monte Carlo collision code oopd1 to explore the spatio-temporal evolution of the electron heating mechanism with pressure in a capacitively coupled oxygen discharge including and excluding the detachment by the singlet molecular metastable states. We find that detachment by the singlet metastable state $O_2(b^1\Sigma_g^+)$ has significant effect while $O_2(a^1\Delta_g)$ has somewhat less significant influence on the discharge properties. We conclude that it is essential to include detachment by both the metastable states. Including the detachment processes has a strong influence on the effective electron temperature and electronegativity in the oxygen discharge, both of these parameters are significantly lower when the detachment processes are included in the simulation. However, it has to be kept in mind that the wall quenching probability for each of the molecular metastable state has a significant influence on the overall discharge and the actual values of the electronegativity and the effective electron temperature. At 10 mTorr, using the full reaction set, the time averaged electron heating displays mainly contribution from ohmic heating in the plasma bulk (the electronegative core) and at higher pressures there is no ohmic heating in the plasma bulk and electron heating in the sheath regions dominates.

ACKNOWLEDGMENTS

This work was partially supported by the Icelandic Research Fund Grant Nos. 130029 and 163086, and the Swedish Government Agency for Innovation Systems (VINNOVA) contract no. 2014-04876.

REFERENCES

- [1] M. W. Kiehbauch and D. B. Graves, *Journal of Vacuum Science and Technology A* **21**, 660–670 (2003).
- [2] J. T. Gudmundsson, *Journal of Physics D: Applied Physics* **37**, 2073–2081 (2004).
- [3] D. A. Toneli, R. S. Pessoa, M. Roberto, and J. T. Gudmundsson, *Journal of Physics D: Applied Physics* **48**, p. 325202 (2015).
- [4] J. T. Gudmundsson, E. Kawamura, and M. A. Lieberman, *Plasma Sources Science and Technology* **22**, p. 035011 (2013).
- [5] J. T. Gudmundsson and M. A. Lieberman, *Plasma Sources Science and Technology* **24**, p. 035016 (2015).
- [6] J. T. Gudmundsson and B. Ventéjou, *Journal of Applied Physics* **118**, p. 153302 (2015).
- [7] V. A. Godyak and R. B. Piejak, *Physical Review Letters* **65**, 996–999 (1990).

- [8] V. Vahedi, C. K. Birdsall, M. A. Lieberman, G. DiPeso, and T. D. Rognlien, *Plasma Sources Science and Technology* **2**, 273–278 (1993).
- [9] S. Huang and J. T. Gudmundsson, *Plasma Sources Science and Technology* **22**, p. 055020 (2013).
- [10] H. Hannesdottir and J. T. Gudmundsson, *Plasma Sources Science and Technology* **25**, p. 055002 (2016).
- [11] F. X. Bronold, K. Matyash, D. T. R. Schneider, and H. Fehske, *Journal of Physics D: Applied Physics* **40**, 6583–6592 (2007).
- [12] A. Derzsi, T. Lafleur, J.-P. Booth, I. Korolov, and Z. Donkó, *Plasma Sources Science and Technology* **25**, p. 015004 (2016).
- [13] E. Kawamura, C. K. Birdsall, and V. Vahedi, *Plasma Sources Science and Technology* **9**, 413–428 (2000).
- [14] A. Midey, I. Dotan, and A. A. Viggiano, *Journal of Physical Chemistry A* **113**, 3040–3045 (2008).
- [15] N. L. Aleksandrov, *Soviet Physics-Technical Physics* **23**, 806–808 (1978).
- [16] R. L. Sharpless and T. G. Slanger, *Journal of Chemical Physics* **91**, 7947 – 7950 (1989).
- [17] B. P. Wood, “Sheath heating in low-pressure capacitive radio frequency discharges,” Ph.D. thesis, University of California, Berkeley 1991.
- [18] D. Vender and R. W. Boswell, *Journal of Vacuum Science and Technology A* **10**, 1331–1338 (1992).
- [19] A. Greb, A. R. Gibson, K. Niemi, D. O’Connell, and T. Gans, *Plasma Sources Science and Technology* **24**, p. 044003 (2015).
- [20] S. Kechkar, “Experimental investigation of a low pressure capacitively-coupled discharge,” Ph.D. thesis, Dublin City University 2015.
- [21] J. Pulpytel, W. Morscheidt, and F. Arefi-Khonsari, *Journal of Applied Physics* **101**, p. 073308 (2007).
- [22] E. Stoffels, W. W. Stoffels, D. Vender, M. Kando, G. M. W. Kroessen, and F. J. de Hoog, *Physical Review E* **51**, 2425 – 2435 (1995).
- [23] K. Bera, S. Rauf, and K. Collins, *AIP Conference Proceedings* **1333**, 1027–1032 (2011).
- [24] M. E. Ryskin and B. R. Shub, *Reaction Kinetics and Catalysis Letters* **17**, 41–46 (1981).
- [25] R. J. O’Brien and G. H. Myers, *Journal of Chemical Physics* **53**, 3832–3835 (1970).